World Journal of Advanced Research and Reviews
eISSN: 2581-9615 CODEN (USA): WJARAI
Cross Ref DOI: 10.30574/wjarr
Journal homepage: https://wjarr.com/

(Research Article)

Check for updates

INFLUENCE OF PUMP PULSE WIDTH ON THE PERFORMANCE OF BRILLOUIN OPTICAL FIBER SENSORS

Diakaridia Sanogo [1, 2, *], Hamidou Tangara [2] and Kossi Aniya Amedome Min-Dianey [3]

[1] *Department of Mechanical and Energy Engineering, National School of Engineering Abderhamane Baba Touré, P.O.Box 242, Bamako-Mali.*
[2] *Department of Electrical Engineering, National School of Engineering Abderhamane Baba Touré, P.O.Box 242, Bamako-Mali.*
[3] *Department of Physics, Faculty of Science, University of Lomé, 01 P.O.Box 1515, Lomé, Togo.*
* Corresponding Author

World Journal of Advanced Research and Reviews, 2026, 31(03), 526–534

Publication history: Received on 01 August 2026; revised on 07 September 2026; accepted on 09 September 2026

Article DOI: https://doi.org/10.30574/wjarr.2026.31.3.2337

ABSTRACT

In this article, we have investigated the influence of pump pulse width on the spatial resolution of optical fiber temperature and strain sensors based on stimulated Brillouin scattering. Pump pulse widths of 2, 5, 10, 20, 50, and 100 ns were used. For pulse widths of 2 and 5 ns, broadening of the Brillouin Gain Spectrum (BGS) is observed. That spectral broadening makes it difficult to estimate the center frequency of the BGS. Conversely, longer pulses (20, 50, or 100 ns) produce narrow spectra and high frequency accuracy, on one hand, and lead to a worse spatial resolution (2, 5, and 10 m), respectively on the other hand. A Pulse width of 10 ns showed an optimal balance between spatial and frequency resolutions. It enabled detection of temperature and/or strain variations of 156°C and 3630 με over 100 m long sensing distance, with uncertainty of only 5.027×10^{-4} °C and 117×10^{-6} με.

Keywords: Sensor, Optical Fiber, Pump Pulse, Brillouin Gain Spectrum (BGS), Brillouin Scattering

1 INTRODUCTION

The rise of fiber optic technologies in recent decades has transformed many sectors, particularly, sensing and measurement. Among these technologies, fiber optic sensors based on the Brillouin effect stand out for their ability to provide highly accurate distributed measurements of temperature and strain [1- 4]. These sensors find applications in diverse fields, including the monitoring of civil engineering infrastructures (bridges, tunnels), pipelines monitoring, and even temperature monitoring on power transmission lines. The Brillouin effect, which arises from the interaction between light and acoustic waves in the fiber, enables the detection of temperature and strain variations by analyzing changes in the frequency of the backscattered signal [5-7]. However, researchers evaluate these sensors based on several key parameters. One of them is the width of the pump pulse used to generate the Brillouin effect. The accuracy of temperature and strain measurements is directly influenced by the pulse width, which plays a key role in determining the spatial resolution and the sensitivity of the sensor [8-11]. Theoretically, the spatial resolution is defined by the pump pulse width. A pulse shorter than 10 ns leads to excessive broadening of the Brillouin gain spectrum bandwidth [12-14]. This broadening, due to a poor signal-to-noise ratio, makes it difficult to estimate the BGS center frequency. Thus, short pulse width severely limits the sensing range [15-17]. A long pulse (few tens of nanoseconds) provides good signal quality, enabling measurements over long distances. On the other hand, a longer pulse width has the disadvantage of providing a poor spatial resolution (m-scale) [18, 19]. This paper studies in detail the influence of the pump pulse width on the spatial resolution, as well as the frequency resolution of Brillouin Optical Time Domain Analysis (BOTDA) sensor [9,10].

2 METHODOLOGY AND PRINCIPLE

The implementation of a BOTDA sensor has been done through numerical simulation using MATLAB. A single-mode silica (SiO_2) optical fiber was used. The measurement fiber, with a total length of 100 m, is arranged as shown in Figure 1. A 99-m fiber (main fiber) is characterized by a Brillouin frequency shift (BFS) of 10.850 GHz. At the far end of the main fiber, a 1-m length of another type of single-mode silica fiber with a BFS of 11.025 GHz serving as perturbation was inserted. The perturbation could be a temperature rise or even a mechanical stress inducing a BFS variation. The temperature and strain coefficient of the chosen measurement fiber are 1.12 MHZ/°C and 0.0482 MHz/με, respectively.

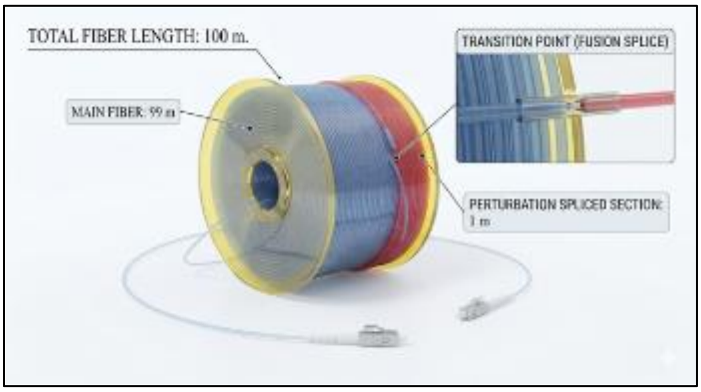

Figure 1: Fiber organization

The measurement principle is that of standard BOTDA [20]. As shown in Figure 2, a pump pulse is coupled with laser 1 in the near end of the fiber under test (FUT) through a three-port circulator, while a continuous wave (CW) is directed into the far end by laser 2. A traveling virtual sensor is created by Stimulated Brillouin Scattering (SBS) as the pump pulse interacts with acoustic phonons in the lattice. Energy is transmitted between the two light waves (Brillouin gain or loss) when the frequency difference between the pump and probe is equal to the local BFS [21]. Using the constant speed of light in the fiber, the precise physical position along the fiber is ascertained by measuring the time delay of the returning and interacting signals. Changes in the local temperature and mechanical stress (compression or stretching) of the fiber cause a linear change in the Brillouin frequency shift. The system obtains a full Brillouin profile throughout the whole fiber length by sweeping the frequency difference.

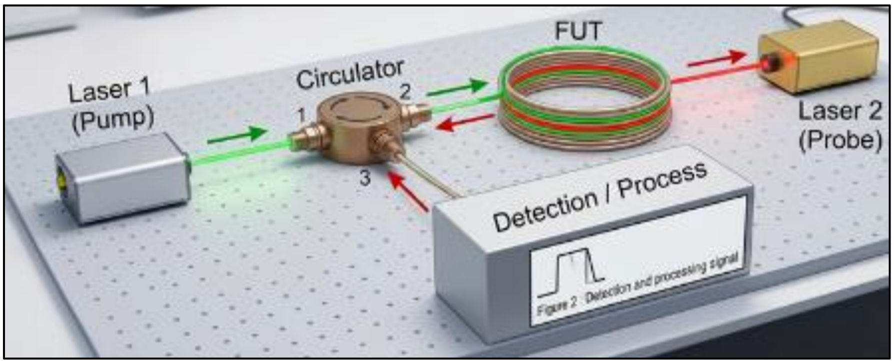

Figure 2: Principle of BOTDA

To simulate BOTDA sensor, the well-known three coupled wave equations (pulsed pump, continuous probe, and acoustic wave) were employed to model the interaction between optical and acoustic waves [22]. These equations are as follows:

Optical field (E_L) pump equation:

$$\frac{\partial E_L}{\partial z} + \frac{n}{c}\frac{\partial E_L}{\partial t} = -\alpha E_L - \frac{g}{2}|E_S|^2 E_L - K_P E_S \quad \text{(Eq. 1)}$$

Stokes (E_S) Equation:

$$\frac{\partial E_S}{\partial z} - \frac{n}{c}\frac{\partial E_S}{\partial t} = -\alpha E_S - \frac{g}{2}|E_L|^2 E_S - K_P^* E_L \quad \text{(Eq. 2)}$$

Acoustic wave ρ:

$$\frac{\partial \rho}{\partial t} + \frac{\rho}{\tau} = \Gamma |E_L|^2 |E_S|^2 \quad \text{(Eq. 3)}$$

Where E_L, E_S and ρ stand for pump pulse, Continuous Wave (CW) and acoustic wave, respectively. Kp and Kp*, are constants, Γ: acoustic damping coefficient; g: Brillouin gain profile.

The gain is modeled as a Gaussian function of the frequency:

$$g_\omega(f) = \exp\left(-\frac{(f - f_B)^2}{2(\Delta f_B)^2}\right) \quad \text{(Eq. 4)}$$

With $g_\omega(f)$: Brillouin gain coefficient; f_B: Brillouin frequency shift.

A higher-power laser pulse is sent into the near end of the fiber. This pulse, commonly called a "pump," interacts with the silica that make up the fiber and generates acoustic waves. A virtual moving sensor that travels along the entire length of the fiber is thus created. At the opposite end of the fiber, CW "probe" light with a specific wavelength is continuously injected. When the "moving" sensor scans a region of the fiber that exhibits the temperature/strain characteristics tested by the specific CW probe wavelength used, the probe light is perturbed by stimulated Brillouin amplification. The perturbed light is then analyzed in the time domain to locate the position and length of the perturbed region along the fiber.

3 RESULTS AND DISCUSSIONS

3.1 Pump Pulse Width and Spatial Resolution

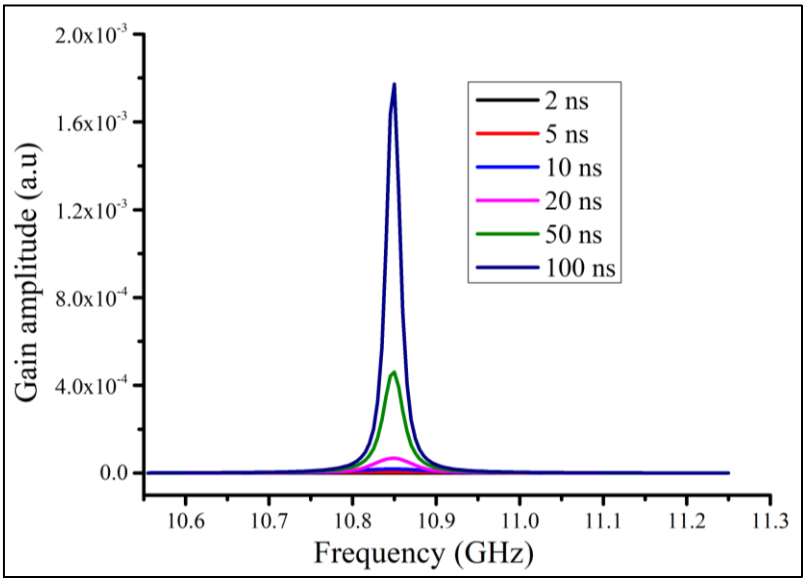

Figure 3: Frequency spectra for different pulse durations

To study the influence of pump pulse width on Brillouin signal quality, we used different pulse widths. Figure 3 shows the Brillouin gain spectra (BGS) acquired using 2, 5, 10, 20, 50, and 100 ns pump pulses. The choice of these pulse widths was not arbitrary. Indeed, we considered 10 ns as a critical value of pulse width. This is because the acoustic phonons generated in the fiber have a lifetime of 10 ns. This minimum time between consecutive pulses is therefore necessary to obtain a good quality Brillouin signal. When a pulse width smaller than 10 ns is used, the acoustic waves created by a pulse do not have enough time to completely vanish before the arrival of those generated by the next pulses. This leads to a spectral overlap of acoustic waves from successive pulses. The Brillouin signal obtained under these conditions will be of poor quality. The signal amplitude will drop drastically, resulting in a broadening of the gain spectrum and making it difficult to determine the BGS center frequency. Figure 3 shows that for pulse widths of 2 ns (black spectrum) and 5 ns (red spectrum), the amplitude of the Brillouin signal is low. For these pulses, the signal is practically indistinguishable from the noise. It begins to be visible at 10 ns (blue spectrum). Conversely, for 20 ns (pink spectrum), 50 ns (green spectrum), and 100 ns (blue dotted spectrum), the signal amplitude is high.

We investigated the effect of pump pulse width on the Brillouin gain spectrum by performing simulations with pulse widths of 2, 5, 10, 20, 50, and 100 ns. Figure 4 shows the normalized gain spectra for different pulse widths.

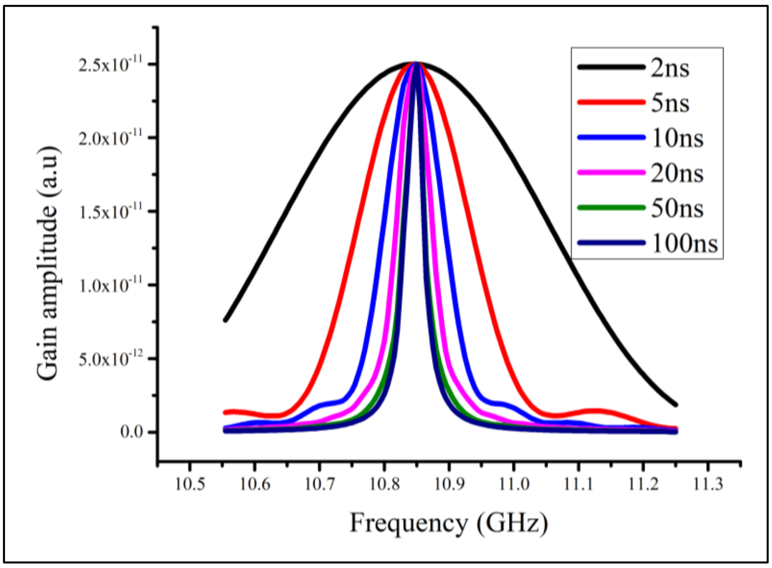

Figure 3: Normalized frequency spectra for pulse durations of: 2 ns (black), 5 ns (red), 10 ns (blue), 20 ns (pink), 50 ns (green), and 100 ns (dark blue)

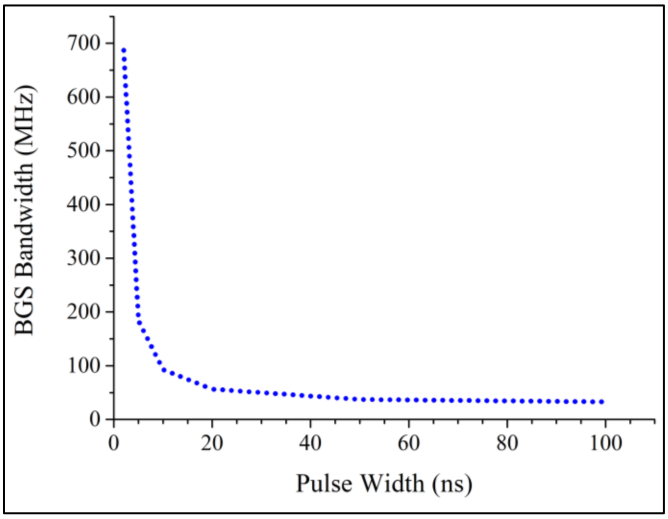

Figure 4: Pump pulse duration as a function of BGS line width

It is apparent that for longer pulse durations (a few tens of ns), the BGS is narrow (on the order of a few tens of MHz). However, it becomes wider when pulses shorter than 10 ns are used. The BGS linewidth even reaches 687 MHz for a pulse width of 2 ns (black spectrum). It is worth noting that the gain spectrum broadens and its shape looks like a Gaussian rather than its original Lorentzian profile when the pump pulse duration falls below the lifetime of acoustic phonons (10 ns).

Figure 5 highlights the relationship between the pump pulse width and the Brillouin gain spectrum bandwidth. It is clear that for pulses setting from 50 to 100 ns, the BGS width is within the bandwidth of stimulated Brillouin scattering (27–30 MHz) [4], while it starts to broaden from 37 to 92 MHz when the pulse widths decrease from 50 to 10 ns. The Brillouin gain spectrum undergoes excessive broadening, reaching values of 183 even 687 MHz when the pulse duration is 5 and 2 ns, respectively. One important remark is that the result of the numerical simulation is in perfect agreement with the theoretical analysis. Since the spatial resolution is defined by the pulse duration, it is difficult to obtain a resolution better than 1 m in the standard BOTDA scheme due to spectral broadening.

We observe that the bandwidth varies considerably with the pulse width. For very short pulses, such as 2 ns and 5 ns, the bandwidth is extremely wide (687.13 MHz and 183.35 MHz, respectively), which is detrimental to the quality of the signal and complicates measurements while negatively affecting the sensor's spatial resolution. Increasing the pulse width results in a significant reduction in the bandwidth. It decreases from 92.82 MHz for 10 ns to 56.55 MHz for 20 ns, and reaches lower values, such as 32.90 MHz for 100 ns. The measurement error follows a similar trend. It is particularly high for short pulses (4.56×10^{-3} MHz for 2 ns), reflecting not only the limitations due to bandwidth but also the poor quality of the Brillouin signal. From 10 ns onward, the error decreases significantly, reaching 4.933×10^{-4} MHz, and continues to decrease to 1.219×10^{-4} MHz at 100 ns. This confirms that longer pulses allow for more precise measurements.

It is important to note that a larger pulse width, while improving accuracy, reduces spatial resolution. Thus, 100 ns pulses, although very precise, are not suitable for detecting centimeter-scale defects. Conversely, a 10-ns pulse width produces a broad spectrum with a center frequency that is difficult to identify. Under these circumstances, the latter is estimated with a large margin of error, thus making the measurements unreliable. However, beyond 10 ns, the measurements become more precise, thanks to the narrowing BGS spectral width.

3.2 Pump Pulse Width and Measurement Error

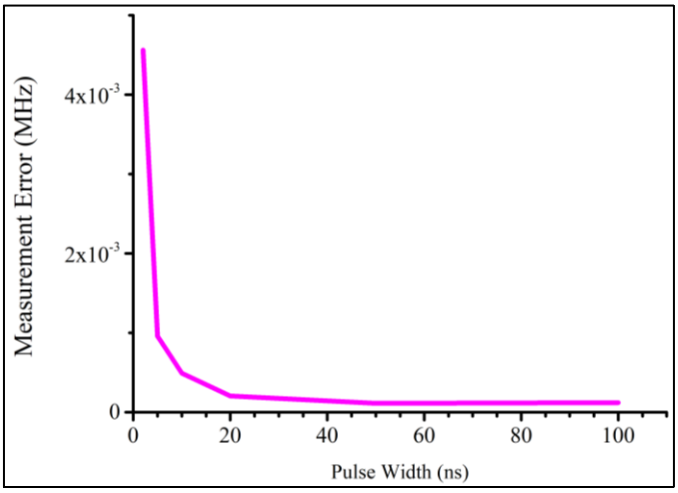

Figure 5: Pump pulse widths as function of measurement errors

Figure 6 reports pump pulse widths as a function of measurement uncertainties. It can be seen that a shorter pulse width leads to a higher measurement error. As the pulse width increases progressively, a significant error decrease is observed. For a pulse width of 10 ns, the error is 4.933×10^{-4} MHz. The error then decreases from 2.050×10^{-4} MHz for 20 ns to 1.219×10^{-4} MHz for 100 ns. This result can be explained by the fact that a large pulse width allows for better resolution and increased accuracy, thus reducing measurement uncertainty. In order to minimize measurement errors, it is better to use a minimum pulse width of 10 ns. For pulse widths of 2 and 5 ns, spectral broadening is observed leading to inaccuracies in the localization of the BGS center frequency. Conversely, pulse widths of 20, 50 and 100 ns offer narrow linewidth spectra, thus improving measurement accuracy. It should be noted that the measurement uncertainty decreases in inverse proportion to the pulse width. The results show a clear trade-off between spatial resolution and spectral accuracy. A shorter pump pulse leads to poor spatial resolution, poor measurement accuracy, and a limited measurement range. Conversely, a long pulse width (100 ns), in addition to allowing measurements over long distances, provides excellent measurement accuracy but gives poor spatial resolution (10 m).

3.3 Detecting 1 m perturbation with a 20-cm spatial resolution sensor

To simulate this sensor, a 2-ns pump pulse, corresponding to 20 cm spatial resolution was coupled into 100 m of single-mode fiber to locate a 1-m segment of disturbance. The 3D Brillouin gain spectrum reconstructed along the entire measurement length is shown in Figure 7a. A close-up view of the last 5 m is shown in Figure 7b. A shift towards higher frequencies is observed in the spectrum at the 96th m. However, the shifted portion is not completely distinguishable from the rest of the spectrum. This implies that the spatial resolution of the sensor is not suitable for efficiently resolving the disturbance located at the far end of the fiber. Figure 7a illustrates the 3D BGS constructed along the measurement fiber. It can be remarked that the spectrum is uniform, but the signal quality is poor. A zoom of the last 5 m is shown in Figure 7b. A shift towards higher frequencies is observed between the 96th and 97th m. However, the shifted spectrum does not stand out as clearly from the main spectrum. Therefore, it becomes difficult to determine the peak frequency accurately. Figure 7c shows the measured spectrum and its Lorentz curve fit. A broadening of the gain spectrum is observed due to the poor signal quality. This feature compromises the efficient localization of the peak frequency. The 20-cm theoretical spatial resolution, defined by the 2-ns pulse duration, is ideal for detecting disturbances on the order of centimeters. However, the broadening of the spectrum makes it difficult to determine the exact BGS peak frequency. This thereby limits the frequency accuracy. Furthermore, the low signal power makes any potential extension of the sensor's measurement range unlikely.

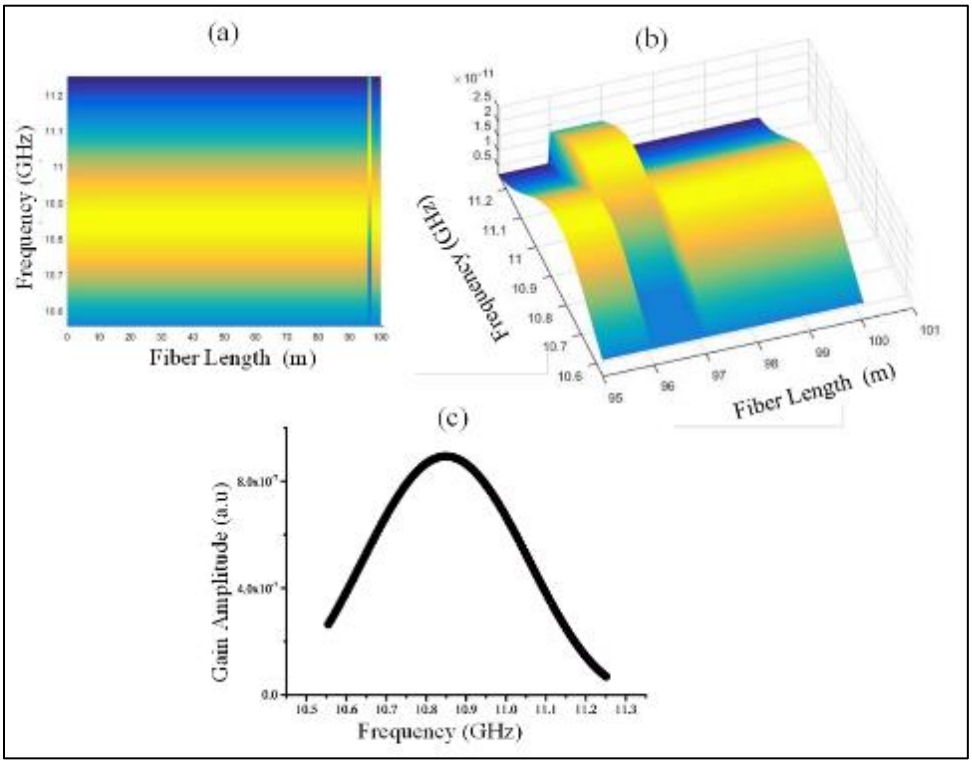

Figure 6: Gain spectrum: (a), 3D over the entire measurement length; (b), a zoom on the last 5 m of the fiber; (c): measured at the 95th m

3.4 Detecting 1 m perturbation with a 1-m spatial resolution sensor

A 10-ns pulse width is sent into 100 m fiber to locate 1 m segment under perturbation. The 3D Brillouin gain spectrum reconstructed along the measurement fiber is shown in Figure 8a. Figure 8b depicts a zoom on the last 5 m. One can observe an upshifted spectral component located between 96th and 97th m. Moreover, the shifted part of the spectrum is centered at 11.025 GHz, while the rest of the spectrum is centered on the BFS of the main fiber (10.850 GHz). Figure 8c illustrates the BGS measured in the perturbed region. The spectrum appears to be free from any distortion. Its bandwidth is 92.82 MHz, and the center frequency is 11.025 GHz, corresponding to the BFS of the perturbed section. Furthermore, a narrow bandwidth is a useful feature for improving the accuracy of spectrum peak frequency estimation. This demonstrates the sensor's ability to effectively discriminate the 1 m-long disturbance located at the far end of the fiber.

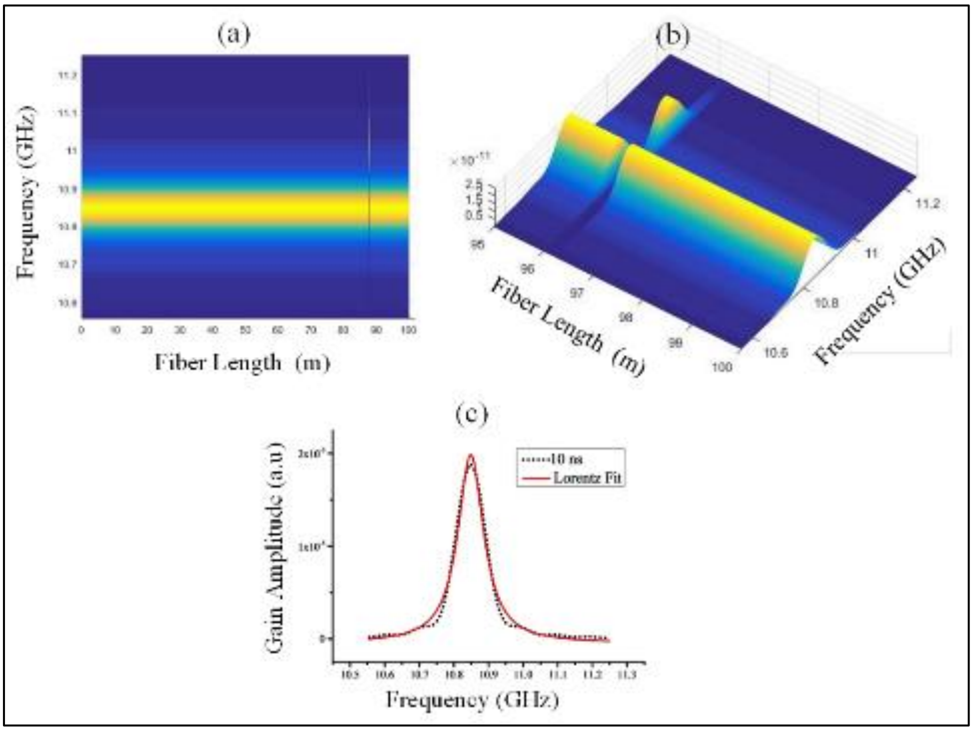

Figure 7: Gain spectrum: (a), in 3D over the entire measurement length; (b), a zoom on the last 5 m of the fiber; (c): BGS measured at the 95th m

To test the detection capability of our sensor, we performed measurements both in the vicinity and inside the inserted fiber section. Figure 9 shows the spectra measured at 95 m (black-solid-line), and the one measured at 96.12 m (red-solid line) inside the perturbed section. The peak frequency of the spectrum measured at 95 m (black-solid-line) is 10.850 GHz with a standard deviation of 4.933×10^{-4} MHz. The spectrum measured at 96.12 m (red-solid line) in the perturbed region is centered at 11.025 GHz, which corresponds to the actual BFS of the inserted fiber section. The standard deviation of the measurement is 5.029×10^{-4} MHz, corresponding to temperature and strain resolutions of 5.63×10^{-4}°C and 24.24×10^{-6} με, respectively. It can be noticed that the BFS difference between the reconstructed spectra is 175 MHz. Knowing that the temperature and strain coefficients of the used fiber are 1.12 MHz/°C and 0.0482 MHz/με [3], respectively, this frequency variation corresponds to a temperature rise of 156 °C and a strain of 3630 με.

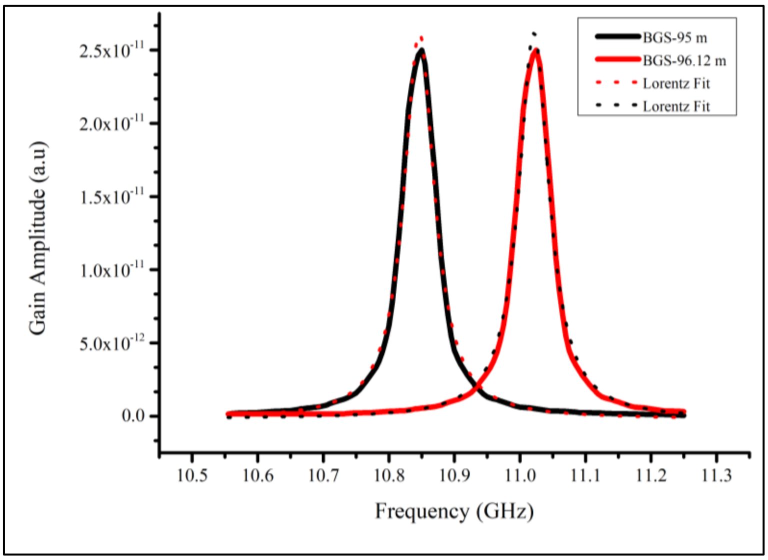

Figure 8: BGS reconstructed: in the vicinity of the perturbed fiber section (black-solid line); in the perturbed section (red-solid line)

4 CONCLUSION

This paper presented an in-depth analysis of the influence of pump pulse width on both the spatial and frequency resolution of fiber optic Brillouin temperature and strain sensors. The work was carried out through numerical simulation using three coupled wave equations (pulsed pump, continuous probe, and acoustic wave) to model the interaction between optical and acoustic waves. Pulses of 2, 5, 10, 20, 50 and 100 ns were used. For pulses shorter than 10 ns (transient regime), a broadening of the Brillouin gain spectrum is observed, making it difficult to estimate its center frequency. In contrast, pulse widths greater than 10 ns allow for narrow spectra and high frequency resolution, at the cost of reduced spatial resolution. Short pulses offer better spatial resolution, while long pulses improve spectral accuracy. These observations are essential for adapting sensors to diverse applications, from precise measurements over long distances to fine detection in localized areas. The 10-ns pulse demonstrated an optimal balance between spatial resolution and spectral accuracy. It enabled the detection of temperature and/or strain variations of 156 °C and 3630 με at the far end of a 100 m long single mode fiber, with uncertainties of 5.027×10^{-4} °C and 117×10^{-6} με, respectively.

STATEMENTS ON COMPLIANCE WITH ETHICAL STANDARDS

Acknowledgments

The authors acknowledge the National School of Engineering for providing the institutional infrastructure, library access, and facilities necessary to complete this research.

Funding Source

This research received no external funding. The work was funded entirely by the authors' personal resources.

Disclosure of conflict of interest

The authors declare no conflicts of interest regarding this manuscript.

REFERENCES

[1] M. Niklès, L. Thévenaz, and P. A. Robert, "Simple distributed fiber sensor based on Brillouin gain spectrum analysis," *Optics Letters*, vol. 21, no. 10, pp. 758–760, May 1996.

[2] Y. Dong, H. Zhang, L. Chen and X. Bao, "2-cm-spatial-resolution and 2-km-range Brillouin optical Fiber Sensor using a transient differential pulse pair," *Appl. Opt.*51 (9), 1229-1235 (2012).

[3] Stella M. Foaleng, Moshe Tur, Jean-Charles Beugnot, and Luc Thévenaz., "High Spatial and Spectral Resolution Long-Range Sensing Using Brillouin Echoes," *JOURNAL OF LIGHTWAVE TECHNOLOGY*, 28(20) 2993-3003 (2010)

[4] Y. Dong, X. Bao and W. Li., "Using Differential Brillouin Gain for Improve the Temperature Accuracy and Spatial Resolution in a Long-distance Distributed Fiber Sensor," *Applied. Optics*. 48, 4297- 4230 (2009).

[5] T. Horiguchi, K. Shimizu, T. Kurashima, M. Tateda, and Y. Koyamada, "Development of a distributed sensing technique using Brillouin scattering," *Journal of Lightwave Technology*, vol. 13, no. 7, pp. 1296–1302, Jul. 1995.

[6] X. Bao and L. Chen, "Recent progress in Brillouin scattering based fiber sensors," *Sensors*, vol. 11, no. 4, pp. 4152–4187, Apr. 2011.

[7] Hiroshi Nasurse and Mitsuhiro Tateda., ''Trade-off between the spatial and frequency resolutions in measuring in measuring the power spectrum of the Brillouin backscattered light in an optical fiber,''. *APPLIED OPTICS*, 38(31), 6516~6521 (2000);

[8] Hiroshi Nasurse and Mitsuhiro Tateda., ''Launched pulse-shape dependence of the power spectrum of the spontaneous Brillouin backscattered light in an optical fiber,'' *APPLIED OPTICS*, 39(34), 6376~6384 (2000);

[9] L. Thévenaz, "Brillouin distributed fiber sensors: An overview and applications," *Journal of Sensors*, vol. 2012, Art. no. 204121, Oct. 2012.

[10] A. Loayssa, R. Ruiz-Lombera, and J. Urricelqui, "Review of high-performance distributed time-domain sensors based on Brillouin scattering," *Sensors*, vol. 15, no. 11, pp. 29332–29362, Nov. 2015.

[11] T. Kurashima, T. Horiguchi, and M. Tateda, "Pulse width dependence of Brillouin frequency in single mode optical fibers," *Optics Express*, vol. 13, no. 23, pp. 9472–9478, Nov. 2005.

[12] A. Yeniay, J.-M. Delavaux, and J. Toulouse, "Spontaneous and stimulated Brillouin scattering spectra and thresholds in SMF-28 optical fiber," *Journal of Lightwave Technology*, vol. 20, no. 8, pp. 1425–1432, Aug. 2002.

[13] L. Rossi, "New Methods for Brillouin Optical Time Domain Analysis," Ph.D. dissertation, Dept. Elect. Eng., Univ. of Bologna, Bologna, Italy, 2021.

[14] J. Jiang et al., "Distributed optical fiber sensing with Brillouin Optical Time Domain Analysis under transient acoustic regimes," *Optics & Laser Technology*, vol. 98, pp. 150–156, Jan. 2018.

[15] S. M. Foaleng, F. Rodriguez-Barrios, S. Martin-Lopez, M. Gonzalez-Herraez, and L. Thévenaz, "Detrimental transient effects in coded Brillouin optical time-domain analysis sensors," *Optics Express*, vol. 19, no. 26, pp. B410–B417, Dec. 2011.

[16] M. J. de Guia, E. Rivera-Prado, and A. Loayssa, "Analytical expression and experimental validation of the Brillouin gain spectral broadening at any sensing spatial resolution," *IEEE Photonics Journal*, vol. 9, no. 3, pp. 1–9, Jun. 2017.

[17] G. P. Agrawal, *Nonlinear Fiber Optics*, 6th ed. San Diego, CA, USA: Academic Press, 2019. *(Chapitre dédié à la diffusion Brillouin stimulée)*.

[18] M. N. Alahbabi, Y. T. Cho, and T. P. Newson, "Modeling and evaluating the performance of Brillouin distributed optical fiber sensors," *Optics Engineering*, vol. 44, no. 6, Art. no. 064401, Jun. 2005.

[19] I. B. Soltani et al., "Effects of Chromatic Dispersion on BOTDA Sensor," *Photonics*, vol. 12, no. 7, Art. no. 726, Jul. 2025.

[20] V. Lecoeuche, S. Randoux, B. Ségard, and J. Zemmouri, "Dynamics of a Brillouin fiber laser: From steady state to chaos," *Physical Review A*, vol. 53, no. 4, pp. 2822–2831, Apr. 1996.

[21] Z. Shi, S. Wang, and X. Zhang, "A long pulse bidirectional BOTDA technology developed for strain positioning and measurement," *Optics & Laser Technology*, vol. 143, Art. no. 107321, Nov. 2021.

[22] Sanogo Diakaridia, Yue Pan, Pengbai Xu, Dengwang Zhou, Benzhang Wang, Lei Teng, Zhiwei Lu, Dexin Ba, And Yongkang Dong "Detecting cm-scale hot spot over 24-km-long single-mode fiber by using differential pulse pair BOTDA based on double-peak spectrum" *OPTICS EXPRESS,* 17727, Vol. 25, No. 15,24 Jul 2017.